Self-Assembly of Amphiphilic Homopolymers Grafted to Spherical Nanoparticle: Complete Embedded Minimal Surfaces and Machine Learning Algorithm for their Recognition

D. A. Mitkovskiy[a,b], A. A. Lazutin[a], A. L. Talis[a], V. V. Vasilevskaya[a,c] *

[a]*A.N. Nesmeyanov Institute of Organoelement Compounds Russian Academy of Sciences, Vavilova ul. 28, bld. 1, 119334, Moscow, Russia*
[b]*Faculty of Fundamental Physical and Chemical Engineering, Lomonosov Moscow State University, Moscow, 119991 Russia*
[c]*Faculty of Chemistry, Lomonosov Moscow State University, Moscow, 119991 Russia*

*e-mail: vvvas@polly.phys.msu.ru

Supplementary Information

Table S1 Geometric symbols

$\mathbf{E^3}$	3D Euclidean space
$\mathbf{E^4}$	Four dimension 4D Euclidean space
$\mathbf{S^2}$	2D (usual) sphere in $\mathbf{E^3}$
$\mathbf{S^3}$	3D sphere in 4D Euclidean space $\mathbf{E^4}$
$\mathbf{H^2}$	2D hyperbolic planes embedded in Euclidean space $\mathbf{E^3}$
W	Weierstrass representations

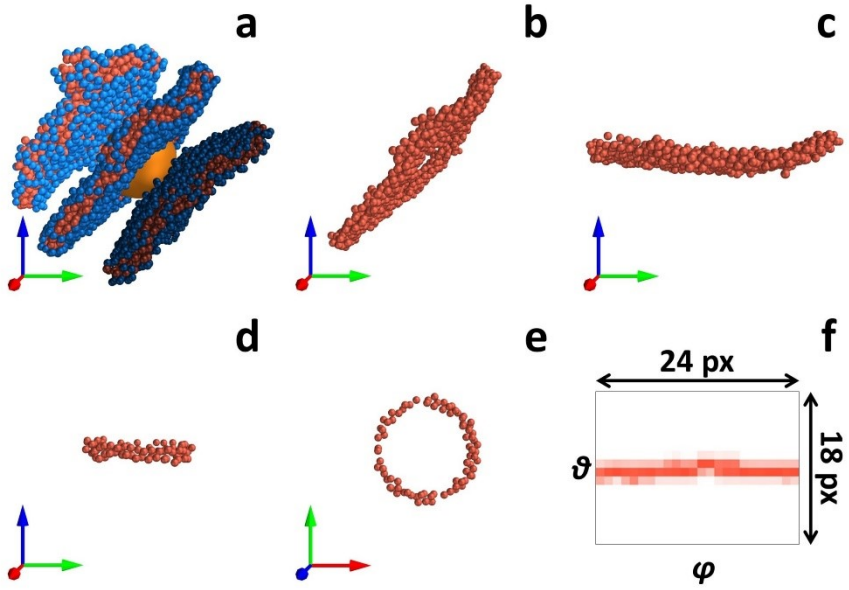

Figure S1. Sequence of data preparation for machine learning algorithm using Costa structure as an example: DBSCAN clustering of the structure into separate elements (a), selecting the central layer of an element (b), element alignment by bringing its inertia tensor to the principal axes (c), grafting points side view (d) and top view (e), grafting points representation as planar 24x18 pixel image in spherical coordinates θ and φ.

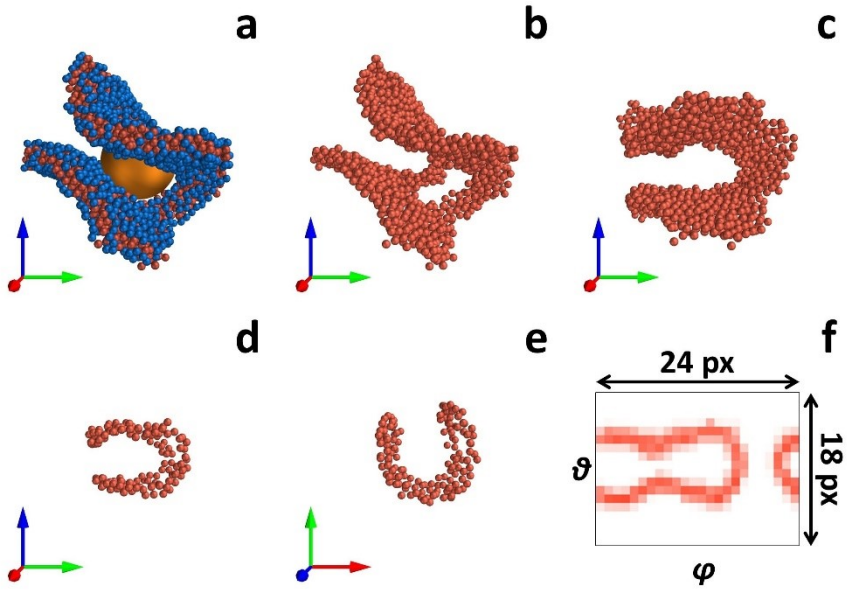

Figure S2. Sequence of data preparation for machine learning algorithm using Enneper structure as an example: DBSCAN clustering of the structure into separate elements (a), selecting the central layer of an element (b), element alignment by bringing its inertia tensor to the principal axes (c), grafting points selecting side view (d) and top view (e), grafting points representation as planar 24x18 pixel image in spherical coordinates θ and φ.

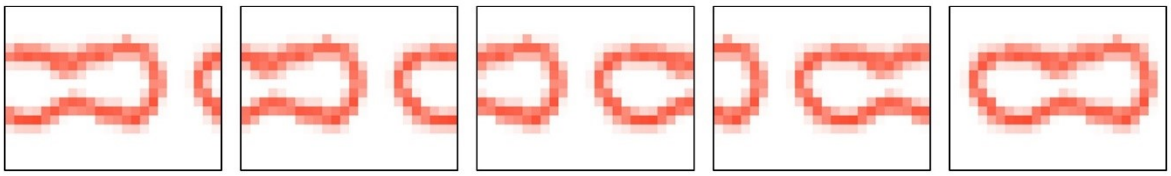

Figure S3. Image augmentation: horizontal sequential transferring 1/5th of the image from the left side to the right side 5 times.

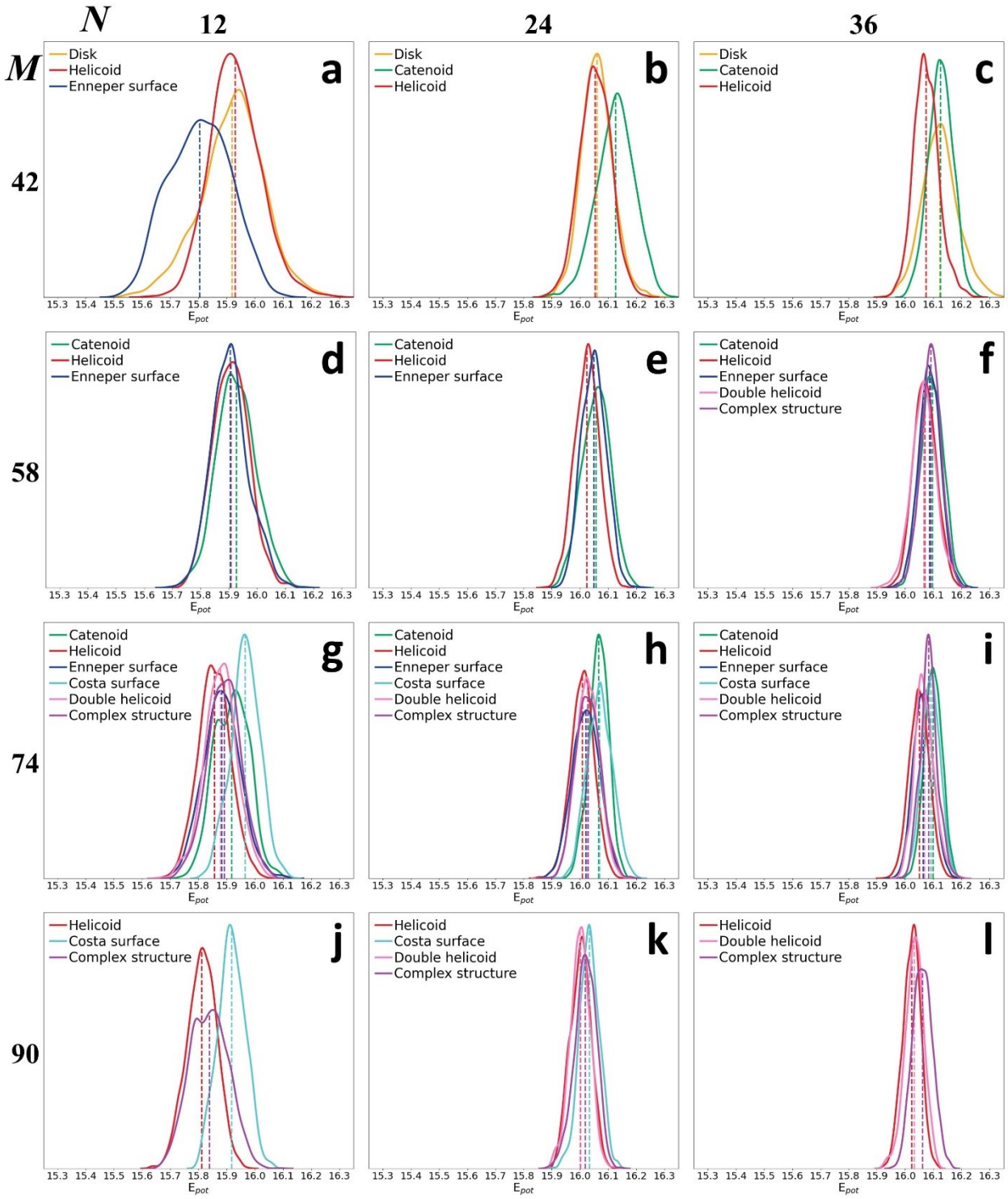

Figure S4. Additional data to Figures 10 for Energy distributions for different structures at different N and M. M = 42, N = 12 (a), 24 (b), 36 (c). M = 58, N = 12 (d), 24 (e), 36 (f). M = 74, N = 12 (g), 24 (h), 36 (i). M = 90, N = 12 (j), 24 (k), 36 (l). Average values $\langle E_{pot} \rangle$ are shown with dashed lines in corresponding colors.

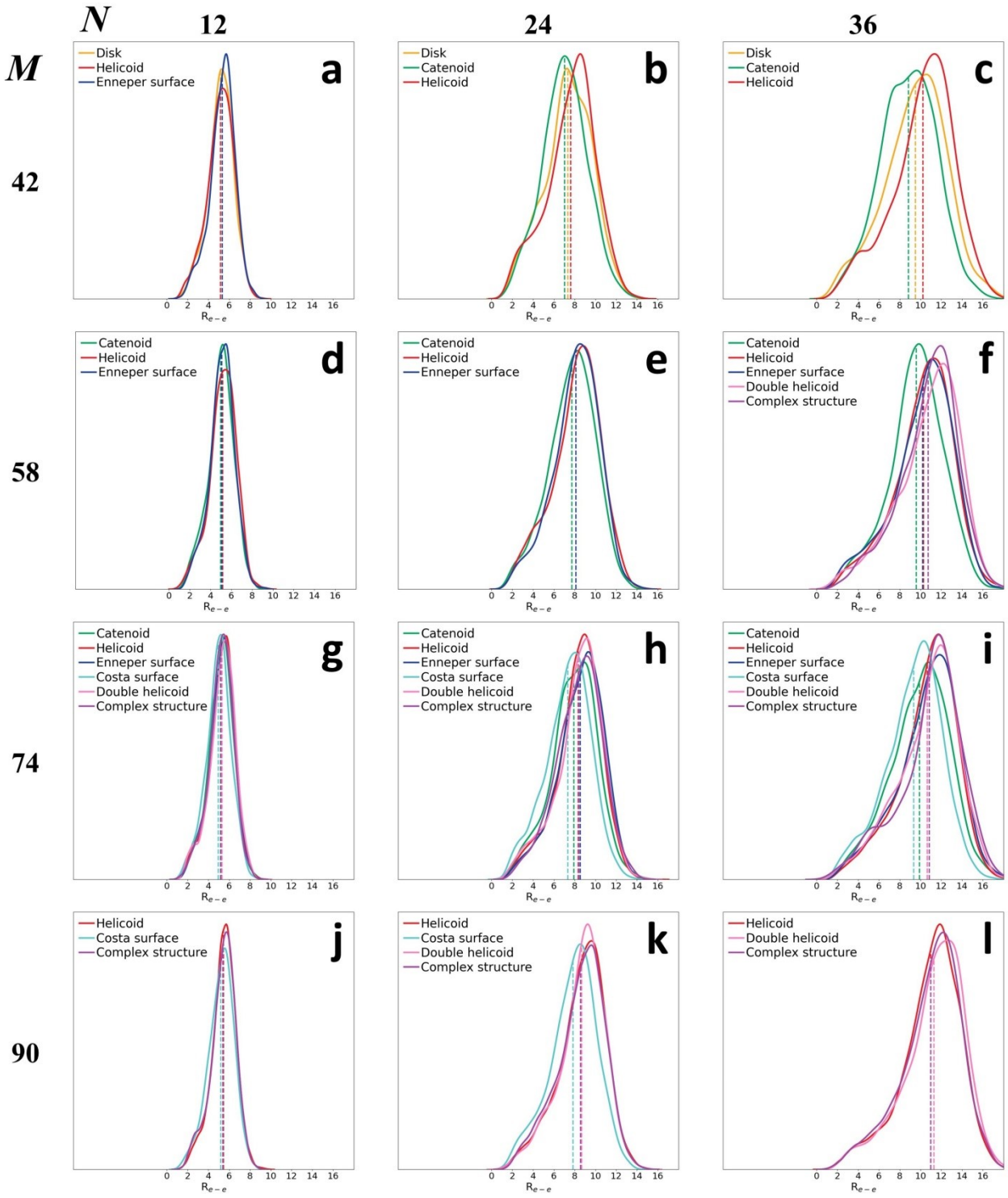

Figure S5. Additional data to Figures 11 for end-to-end distance distributions for different structures at different N and M. M = 42, N = 12 (a), 24 (b), 36 (c). M = 58, N = 12 (d), 24 (e), 36 (f). M = 74, N = 12 (g), 24 (h), 36 (i). M = 90, N = 12 (j), 24 (k), 36 (l). Average values $< R_{e\text{-}e} >$ are shown with dashed lines in corresponding colors.

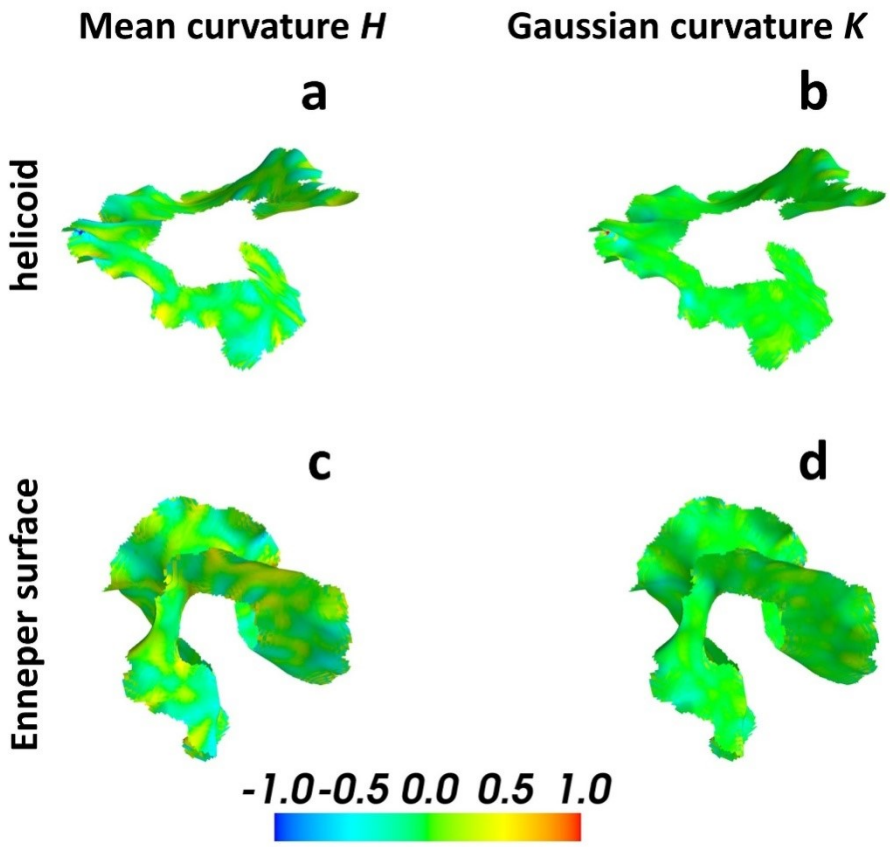

Figure S6. Constructed surfaces for helicoid (M=50, N=24) (a, b) and Enneper structures (M= 58, N=12) (c, d), colored according to calculated local values of mean H (a, c) and Gaussian K (b, d) curvature. The color scale is shown at the bottom of each drawing.